Research Article | Vol. 8, No. 7 | 1 Jul 2018 | OPTICAL MATERIALS EXPRESS 1951
Optical Materials EXPRESS

Holographic performance of silicon polymer films based on photoswitchable molecules

Bjoern Bourdon,[1,2] Sergej Bock,[1,3] Christian Kijatkin,[1,2] Alexandr Shumelyuk,[4] and Mirco Imlau[1,2,*]

[1]*Department of Physics, Barbarastrasse 7, Osnabrueck University, D-49076 Osnabrueck, Germany*
[2]*Center for Cellular Nanoanalytics, Barbarastrasse 11, Osnabrueck University, D-49076 Osnabrueck, Germany*
[3]*Faculty of Electrical Engineering and Information Technology, South Westphalia University of Applied Sciences, Haldener Strasse 182, D-58095 Hagen, Germany*
[4]*Institute of Physics, National Academy of Sciences, 03650 Kyiv, Ukraine*
[*]*mirco.imlau@uni-osnabrueck.de*

Abstract: Holographic silicon polymer films based on photoswitchable molecules are studied with respect to their performance for hologram recording, with photoswitchable ruthenium sulfoxide complexes as an example. Our systematic study reveals that it is possible to record elementary holographic lossy gratings with outstanding quality with respect to their dynamics and in- and off-Bragg read-out features. Furthermore, the possibility for the recording of multiple holograms within the same volume element via angular multiplexing as well as the recording with continuous-wave and a fs-laser pulse train is successfully demonstrated. At the same time, a strong limitation of the maximum diffraction efficiency in the order of $\sim 10^{-3}$ is found that cannot be counterbalanced by either the tuning of material (thickness, concentration, ...) or recording parameters (repetition rate, wavelength, ...). This limitation – being severe for any type of holographic applications – is discussed and compared with the performance of high-efficient single-crystalline reference holographic media. We conclude that the potential of sulfoxide compounds may be hidden in holography until it becomes possible to synthesize polymer films with appropriate three-dimensional structural arrangement of the photoswitchable compounds.

OCIS codes: (090.2900) Optical storage materials; (090.7330) Volume gratings; (160.4330) Nonlinear optical materials; (160.5335) Photosensitive materials; (190.4380) Nonlinear optics, four-wave mixing (190.7110) Ultrafast nonlinear optics.

References and links

1. Th. Woike, W. Krasser, P. S. Bechthold, and S. Haussühl, "Extremely Long-Living Metastable State of $Na_2[Fe(CN)_5NO]\cdot 2H_2O$ Single Crystals: Optical Properties," Phys. Rev. Lett. **53**(18), 1767–1770 (1984).
2. Th. Woike, W. Krasser, and S. Haussühl, "Optical switch, especially for information storage and retrieval," U. S. Patent 4713795 (1987).
3. Th. Woike, W. Kirchner, G. Schetter, T. Barthel, K. Hyung-sang, and S. Haussühl, "New information storage elements on the basis of metastable electronic states," Opt. Commun. **106**(1–3), 6–10 (1994).
4. V. Dieckmann, S. Eicke, K. Springfeld, and M. Imlau, "Transition Metal Compounds Towards Holography," Materials. **5**(6), 1155–1175 (2012).
5. L. Cao, Z. Wang, S. Zong, S. Zhang, F. Zhang, and G. Jin, "Volume holographic polymer of photochromic diarylethene for updatable three-dimensional display," J. Polym. Sci. Pol. Phys. **54**(20), 2050–2058 (2016).
6. R. Häussler, Y. Gritsai, E. Zschau, R. Missbach, H. Sahm, M. Stock, and H. Stolle, "Large real-time holographic 3D displays: enabling components and results," Appl. Opt. **56**(13), F45–F52 (2017).
7. J. J. Rack, "Photoinduced molecular switches," U.S. Patent 6433270 (2002).
8. B. A. McClure and J. J. Rack, "Isomerization in Photochromic Ruthenium Sulfoxide Complexes," Eur. J. Inorg. Chem. **2010**(25), 3895–3904 (2010).
9. V. Dieckmann, S. Eicke, J. J. Rack, Th. Woike, and M. Imlau, "Pronounced photosensitivity of molecular $[Ru(bpy)_2(OSO)]^+$ solutions based on two photoinduced linkage isomers," Opt. Express **17**(17), 15052–15060 (2009).
10. V. Dieckmann, K. Springfeld, S. Eicke, M. Imlau, and J. J. Rack, "Thermal stability, photochromic sensitivity and optical properties of $[Ru(bpy)_2(OSOR)]^+$ compounds with R = Bn, BnCl, BnMe," Opt. Express **18**(22), 23495–23503

#330430 https://doi.org/10.1364/OME.8.001951
Journal © 2018 Received 26 Apr 2018; revised 30 May 2018; accepted 31 May 2018; published 26 Jun 2018

Optical Materials EXPRESS

(2010).
11. K. Springfeld, V. Dieckmann, and M. Imlau, "High-contrast, high-resolution photochromic silicone polymer based on photoswitchable $[Ru(bpy)_2OSO]PF_6$ building blocks," Photonics Res. **1**(4), 197–201 (2013).
12. V. Dieckmann, "Lichtinduzierte Isomerisierung in Sulfoxid- und Nitrosyl-Komplexen: Photosensitivität und Modifikation," Ph.D. thesis, Osnabrueck University, Osnabrueck, Germany (2010).
13. K. Springfeld, "Photoschaltbare Koordinationskomplexe: Festkörpereinbettung und Schwingungsspektroskopie mit MIR-Femtosekundenpulsen," Ph.D. thesis, Osnabrueck University, Osnabrueck, Germany (2013).
14. M. Y. Livshits and J. J. Rack, "Photorefraction from a Photochromic Soft Material," J. Phys. Chem. C **120**(46), 26459–26464 (2016).
15. M. Imlau, S. Haussühl, Th. Woike, R. Schieder, V. Angelov, R. A. Rupp, and K. Schwarz, "Holographic recording by excitation of metastable electronic states in $Na_2[Fe(CN)_5NO]\cdot 2H_2O$: a new photorefractive effect," Appl. Phys. B **68**(5), 877–885 (1999).
16. E. N. Leith, A. Kozma, J. Upatnieks, J. Marks, and N. Massey, "Holographic Data Storage in Three-Dimensional Media," Appl. Opt. **5**(8), 1303–1311 (1966).
17. D. L. Staebler, W. J. Burke, W. Phillips, and J. J. Amodei, "Multiple storage and erasure of fixed holograms in Fe-doped $LiNbO_3$," Appl. Phys. Lett. **26**(4), 182–184 (1975).
18. M. Imlau, Th. Woike, R. Schieder, and R. A. Rupp, "Holographic recording with orthogonally polarized waves in centrosymmetric $Na_2[Fe(CN)_5NO]\cdot 2H_2O$," EPL **53**(4), 471–477 (2001).
19. K.-M. Voit and M. Imlau, "Holographic Spectroscopy: Wavelength-Dependent Analysis of Photosensitive Materials by Means of Holographic Techniques," Materials. **6**(1), 334–358 (2013).
20. B. A. McClure, N. V. Mockus, D. P. Butcher, D. A. Lutterman, C. Turro, J. L. Petersen, and J. J. Rack, "Photochromic Ruthenium Sulfoxide Complexes: Evidence for Isomerization Through a Conical Intersection," Inorg. Chem. **48**(17), 8084–8091 (2009).
21. D. P. Butcher, A. A. Rachford, J. L. Petersen, and J. J. Rack, "Phototriggered S → O Isomerization of a Ruthenium-Bound Chelating Sulfoxide," Inorg. Chem. **45**(23), 9178–9180 (2006).
22. N. V. Mockus, D. Rabinovich, J. L. Petersen, and J. J. Rack, "Femtosecond Isomerization in a Photochromic Molecular Switch," Angew. Chem. Int. Ed. **47**(8), 1458–1461 (2008).
23. B. A. McClure and J. J. Rack, "Ultrafast Spectroscopy of a Photochromic Ruthenium Sulfoxide Complex," Inorg. Chem. **50**(16), 7586–7590 (2011).
24. T. A. Grusenmeyer, B. A. McClure, C. J. Ziegler, and J. J. Rack, "Solvent Effects on Isomerization in a Ruthenium Sulfoxide Complex," Inorg. Chem. **49**(10), 4466–4470 (2010).
25. H. Kogelnik, "Coupled wave theory for thick hologram gratings," Bell Syst. Tech. J. **48**(9), 2909–2947 (1969).
26. M. Fally, M. Imlau, R. A. Rupp, M. A. Ellabban, and Th. Woike, "Specific Recording Kinetics as a General Property of Unconventional Photorefractive Media," Phys. Rev. Lett. **93**(24), 243903 (2004).
27. G. Borrmann, "Die Absorption von Röntgenstrahlen im Fall der Interferenz," Z. Phys. **127**(4), 297–323 (1950).
28. S. Eicke, "Populations- und Relaxationskinetiken laserangeregter photofunktionaler Ruthenium-Sulfoxid-Komnplexe in hochkonzentrierten Lösungen," Ph.D. thesis, Osnabrueck University, Osnabrueck, Germany (2012).
29. S. Eicke, V. Dieckmann, A. Kruse, K.-M. Voit, M. Imlau, and L. Walder, "Dynamics of the light-induced absorption in photochromic $[Ru(bpy)_2(OSO)]^+$," J. Spectrosc. Dyn. **4**, 6 (2014).
30. P.-A. Blanche, A. Bablumian, R. Voorakaranam, C. Christenson, W. Lin, T. Gu, D. Flores, P. Wang, W.-Y. Hsieh, M. Kathaperumal, B. Rachwal, O. Siddiqui, J. Thomas, R. A. Norwood, M. Yamamoto, and N. Peyghambarian, "Holographic three-dimensional telepresence using large-area photorefractive polymer," Nature. **468**(7320), 80–83 (2010).
31. N. Ishii, T. Kato, and J. Abe, "A real-time dynamic holographic material using a fast photochromic molecule," Sci. Rep. **2**, 819 (2012).
32. H. J. Coufal, D. Psaltis, and G. T. Sincerbox, eds., *Holographic Data Storage*, Springer Series in Optical Sciences (Springer-Verlag, Berlin Heidelberg, 2000).
33. M. Imlau, T. Bieringer, S.G. Odoulov, and Th. Woike, "Holographic Data Storage," in *Nanoelectronics and Information Technology: Advanced Electronic Materials and Novel Devices*, R. Waser, ed. (Wiley-VCH, Weinheim, 2012), 3rd ed., pp. 725–750
34. M. Imlau, R. Schieder, R. A. Rupp, and Th. Woike, "Anisotropic holographic scattering in centrosymmetric sodium nitroprusside," Appl. Phys. Lett. **75**(1), 16–18 (1999).
35. M. A. Ellabban, M. Fally, M. Imlau, Th. Woike, R. A. Rupp, and T. Granzow, "Angular and wavelength selectivity of parasitic holograms in cerium doped strontium barium niobate," J. Appl. Phys. **96**(12), 6987–6993 (2004).
36. H. Brüning, V. Dieckmann, B. Schoke, K.-M. Voit, M. Imlau, G. Corradi, and C. Merschjann, "Small-polaron based holograms in $LiNbO_3$ in the visible spectrum," Opt. Express **20**(12), 13326–13336 (2012).
37. M. Goulkov, D. Schaniel, and Th. Woike, "Pulse recording of thermal and linkage isomer gratings in nitrosyl compounds," J. Opt. Soc. Am. B **27**(5), 927–932 (2010).
38. P. T. Manoharan and W. C. Hamilton, "The Crystal Structure of Sodium Nitroprusside," Inorg. Chem. **2**(5), 1043–1047 (1963).
39. Th. Woike, S. Haussühl, B. Sugg, R. A. Rupp, J. Beckers, M. Imlau, and R. Schieder, "Phase gratings in the visible and near-infrared spectral range realized by metastable electronic states in $Na_2[Fe(CN)_5NO]\cdot 2H_2O$," Appl. Phys. B **63**(3), 243–248 (1996).

Optical Materials EXPRESS

1. Introduction

The approach to use photoswitchable molecular compounds as photofunctional building blocks in holographic materials goes back to the original proposal of Woike et al. [1–3]. The molecular level potentially enables a number of important features within the same material: (i) a high tuning ability of the spectral sensitivity due to targeted substitution of ligands and/or central atoms, (ii) the possibility for enabling a reversible write-read-erase cycle, (iii) a ultra-high (holographic) spatial resolution down to the molecular level, (iv) a cheap and quick synthesis on (v) a large scale, (vi) a good mechanical flexibility, (vii) the possibility for tailored dimensioning, (viii) the possibility for adapting the optical density via concentration optimization, and (ix) the possibility to record with either continuous wave (cw) or fs-laser light pulses [4].

Current potential applications include three-dimensional real-time displays [5, 6] either with large scale or as integrated head-on display. Still, however, holographic media based on photoswitchable compounds are not available commercially. The reasons are manifold and include large costs for laborious molecular crystal growth, large optical damping by fundamental absorption, toxicity, and/or the requirement for liquid-nitrogen temperatures [4].

The photoswitchable compounds of the sulfoxide family here are very promising candidates to overcome the majority of these limitations [7, 8]. Our previous reports have already addressed the unique features of photofunctionality at room temperature [9, 10]. Furthermore, we were able to demonstrate the possibility for embedding ruthenium sulfoxides compounds in a polymer matrix with conserved photochromic response [4]. Based on these pre-investigations, the ability to record elementary gratings with promising features for consumer-market holographic applications was proposed [11]. First inspection of the underlying mechanisms are interpreted as index gratings as a result of a causal connection between absorption and index change via Kramers-Kronig relation [4, 12–14]. The question about a dominating role of refractive index changes based on pronounced changes of the molecular polarization by means of light-induced structural alterations, as it has been verified for the photoswitchable sodium nitroprusside $Na_2[Fe(CN)_5NO]\cdot 2H_2O$ (abbr. SNP) [15], has never been addressed so far.

In this contribution, we focus on the investigation of two sulfoxide representatives embedded into the matrix-like polymer polydimethylsiloxane (abbr. PDMS) [4, 11, 13] by means of established holographic analyzing methods [15]: $[Ru(bpy)_2(OSO)]^+$ (abbr. OSO), where bpy is 2,2'-bipyridine, and the $[Ru(bpy)(biq)(OSO)]^+$ complex (abbr. BIQ), where biq is 2,2'-biquinoline and OSO is 2-methylsulfinylbenzoate. By recording up to four elementary gratings within the sample at room temperature, the isomerization of ruthenium sulfoxides from an applied point of view is analyzed. Special attention is given to the measurement of the kinetics of the diffraction efficiency under in- as well as off-Bragg conditions. For the first time, the multiplexed recording of holograms within the same PDMS volume element by means of in-plane angular multiplexing [16, 17] is demonstrated. Furthermore, pioneering results acquired via exposure to a femtosecond-laser pulse train are shown. While these features point to an outstanding performance of OSO-PDMS and BIQ-PDMS polymer films, a severe limitation of the diffraction efficiency of not more than $\sim 10^{-3}$ is found independent on the experimental conditions.

We discuss these findings in direct comparison with SNP as a single-crystalline reference system, that reveals a similar photofunctionality: Two metastable states $MS_{1,2}$ can be (i) populated in the blue-green spectral range and are (ii) reversibly switched to the ground state with red and near-infrared light. Grating recording has been successfully demonstrated in SNP under illumination with laser light in the blue-green spectral range and at temperatures below 200 K. It is attributed to light-induced structural alterations of the photoadressable N-O-bond which results in large absorption and refraction index changes in the order of $\Delta\alpha \sim 10^3\ m^{-1}$ and $\delta n \sim 10^{-2}$, respectively, and diffraction efficiencies of up to unity [15, 18]. Due to the spectral sensitivity which enables write-read-erase cycles and the possibility to write multiple holograms within the same volume (multiplexing) [15], SNP was analyzed in the context of holographic data storage

Optical Materials EXPRESS

already proposed by Woike et al. in 1984 [1–3]. From the direct comparison of the holographic performance of ruthenium sulfoxide compounds with SNP, it can be concluded that the missing crystallographic order of OSO- and BIQ-compounds within the PDMS matrix is decisive for the lack of a pronounced change of the refractive index, i.e. for a diffraction efficiency that is sufficient for holographic applications.

2. Experimental methods

2.1. Film samples

Photochromic, non-toxic OSO-PDMS and BIQ-PDMS silicon polymers were synthesized according to the procedure introduced by Springfeld et al. [11]. The procedure is adopted for medium-scale film synthesis (> 15 cm^2) with sulfoxide concentrations in a broad range between $c = (0.01 - 0.97)$ mM (OSO-PDMS) and up to $c = (1.86 \pm 0.03)$ mM for BIQ-PDMS. We succeeded in the preparation of films of high optical quality even for large thicknesses between 1 and 3 mm. For the purpose of our systematic investigation, the films were cut into stripes of dimensions 80 mm × 20 mm. Figure 1 shows a photograph of a typical OSO-PDMS sample with a concentration $c = (0.97 \pm 0.03)$ mM and thickness $d = (2.2 \pm 0.1)$ mm as an example. All films exhibit an orange/yellow, translucent color and show a moderate number of surface inclusions (cf. also Ref. [4, 11]).

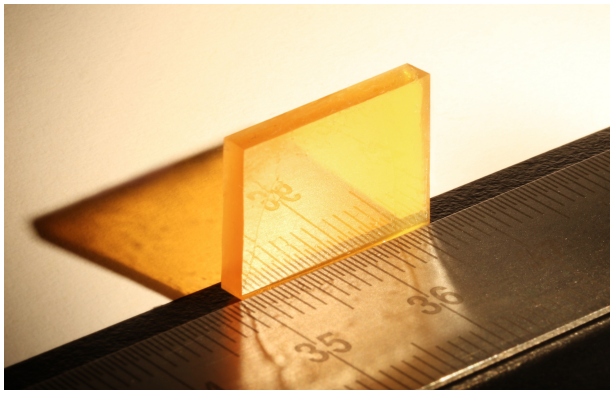

Fig. 1. Photograph of a typical as-prepared OSO-PDMS film sample ($c = (0.97 \pm 0.03)$ mM and thickness $d = (2.2 \pm 0.1)$ mm). The bulky stripe of dimension 17 mm ×13 mm exhibits an orange/yellow, translucent color and shows a moderate number of surface inclusions.

Figure 2 shows the ground state absorption spectra (black lines) of the a) OSO-PDMS and b) BIQ-PDMS samples as used in the experiments of our study. The measurements were performed in relation to a nominally pure PDMS sample of same thickness in the reference path of a two-beam photospectrometer (Shimadzu Scientific Instruments, *UV-3600*).

2.2. Setup for cw-investigations

A self-made two-beam interferometer, schematically depicted in Fig. 3, is applied for the investigation of the as-prepared OSO-silicon polymer films (cf. our technical paper of Ref. [19] for a detailed description). The interferometer is designed for the recording of unslanted elementary holographic gratings with an external Bragg angle of $\Theta_B^{ext} = (4.9 \pm 0.2)°$. Collimated, linearly polarized beams at a measured center wavelength of $\lambda_{record} = (406.6 \pm 0.8)$ nm of a nitride-based semiconductor laser diode (*s*-polarization; type: *iPulse-405-S* from TOPTICA Photonics AG) were used according to the absorption spectrum of the OSO-complex in the ground state (Fig. 2a), and [9, 11, 20]). Careful adjustment of the optical beam paths ensured

Optical Materials EXPRESS

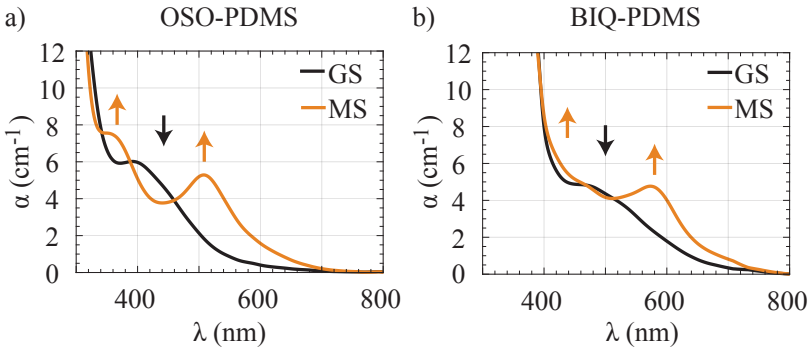

Fig. 2. a) Absorption spectrum of the ground state (GS, black) and metastable state (MS, orange) for OSO embedded in PDMS, concentration $c = (0.36 \pm 0.03)$ mM and thickness $d = (2.1 \pm 0.1)$ mm. b) Absorption spectrum of the ground state (GS, black) and metastable states (MS, orange) for BIQ embedded in PDMS, concentration $c = (1.86 \pm 0.03)$ mM and thickness $d = (1.3 \pm 0.1)$ mm. Orange and black arrows indicate an increase and decrease of the absorption coefficient with respect to the ground state absorption, respectively.

a high-contrast fringe pattern (modulation depth $m = 2\sqrt{I^R \times I^S}/(I^R + I^S) \approx 0.88$ at a total intensity of $I^R + I^S = (19.6 \pm 0.2)$ mW/cm^2, where I^R and I^S are the intensities of the reference and signal beams, respectively).

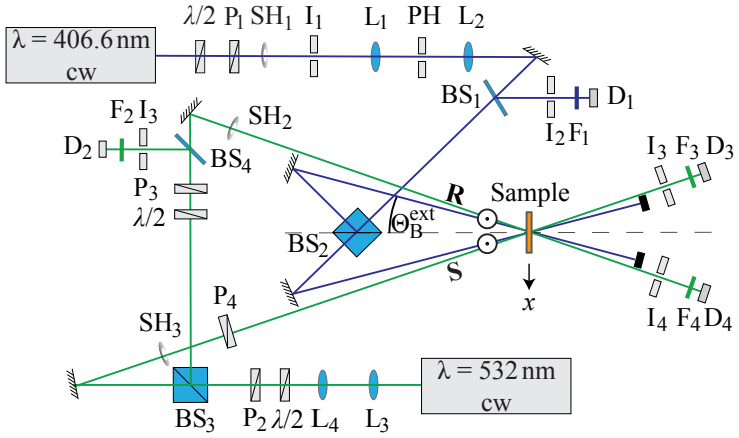

Fig. 3. Experimental setup of our self-made two-beam interferometer. $SH_{1...3}$: shutters, PH: pinhole, $I_{1...4}$: iris diaphragm, $BS_{1...4}$: beam splitters, $D_{1...4}$: diodes, $L_{1...4}$: lenses, $P_{1...4}$: polarizers, $\lambda/2$: half-wave plate, $F_{1...4}$: single line filters, R,S: reference and signal beams. The half angle between the two recording beams at $\lambda_{record} = (406.6 \pm 0.8)$ nm is adjusted to $\Theta_B^{ext} = (4.9 \pm 0.2)°$ that accords with a read-out angle $\Theta^{ext} \approx 6.4°$ at $\lambda_{read} = 532$ nm.

In bright regions, the ultraviolet exposure triggers a Ru d$\pi \rightarrow$ bpy π^* metal-to-ligand-charge-transfer (MLCT) into an S-bonded excited state of the Ru-S-O bond [20–23]. This excited state may relax vibrationally to one of the two O-bonded (Ru-O-S bond) metastable states (MS_1 or MS_2) as schematically depicted in Fig. 4a) (yellow-shaded box). In total, the rise time for the

Optical Materials EXPRESS

formation of MS_1 or MS_2 upon an incident pump pulse is found below 200 ps [20, 23].

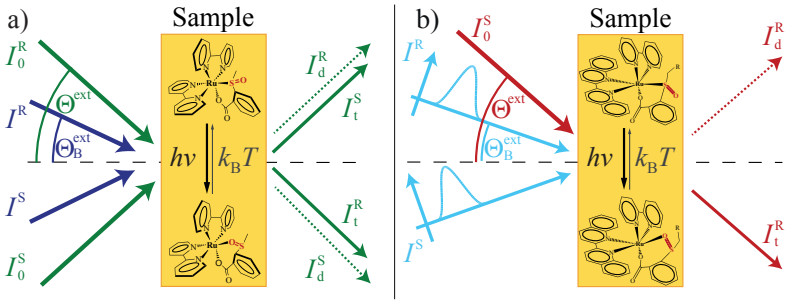

Fig. 4. a) Principal sketch of the incident recording and read-out beam paths with cw-laser light. All intensities were measured with Si-PIN diodes. Furthermore, the light-induced structural changes inside the OSO-complex upon UV/blue light exposure, i.e. the change from a Ru-S-O to a Ru-O-S bond according to Ref. [23], is schematically shown. b) Equivalent principal sketch for fs-pulse recording in BIQ-PDMS polymer films [24].

This photochemical process together with the spatially inhomogeneous exposure results in the appearance of a spatial modulation of the concentration densities $c_{MS_1}(x)$, $c_{MS_2}(x)$. We use in- and off-Bragg-matched read-out in two principle directions both symmetrical with respect to the sample's normal. A continuous-wave laser (frequency-doubled Nd:YAG laser at $\lambda_{read} = 532$ nm, *s*-polarization, type: *Compass 215M-75* from Coherent, Inc.) is applied to probe the temporal evolution $c_{MS_1,MS_2}(x,t)$ via diffraction ($\Theta^{ext} \approx 6.4°$ at 532 nm). According to the models introduced by Imlau et al. [15] and Dieckmann et al. [4], the diffraction process may be attributed to the interaction of the probe beam with either a spatial modulation of density and/or a transmission loss. We note that $MS_{1,2}$ feature a localized alteration of both the atomic and electronic structure. The related broad-band absorption in the visible spectral range [20] (see also absorption spectra of the metastable states in Fig. 2) may be applied for the recording of a spatial modulation of the absorption coefficient, that will appear in-phase with the incident light intensity pattern [4].

The diffraction efficiency $\eta^{R,S} = I_d^{R,S}/I_0^{R,S}$ is applied as key measure in our experimental study [25]. Here, $I_{0,d}^{R,S}$ describe the intensities of incident (0) and first-order diffracted (d) beams, respectively, as depicted in Fig. 4(a)). An influence of the read-out process on the hologram dynamics is suppressed due to small read-out intensities ($I_0^{R,S} = (0.11 \pm 0.01)\,\mathrm{mW/cm^2} \ll I^{R,S}$). Angular-dependent read-out of the diffraction efficiency $\eta(\Delta\Theta^{ext}) = \eta(\Theta^{ext} - \Theta_B^{ext})$ is realized by a high-precision, motorized rotation stage (Newport, type *URM80CC*) at a constant rotation velocity of 0.005°/s. If used for angular multiplexing, the velocity is increased to ≈ 0.01°/s in order to reduce the impact of thermal self-decay of the recorded grating and any influence of the read-out laser.

A similar two-beam interferometer is applied for the study of the film performance under repetitive fs-pulse exposure ($\tau_p \approx 100$ fs, $f_{rep} = 100$ Hz) as schematically depicted in Fig. 5.

Fs-pulses were generated with a standard optical parametric amplifier being pumped by a regeneratively amplified, mode locked Ti:Sapphire laser (*Libra-F HE* and *OPerA Solo*, Coherent, Inc.). It enables adjusting the OPA center wavelength ($\lambda_{record} = 488$ nm) close to the maximum MLCT absorption feature of polymer films with embedded BIQ-molecules (Fig. 2(b)), and [24]) that were used with this setup. The respective photochemical reaction is sketched in Fig. 4(b) (cf. yellow-shaded box). Figure 4(b) also shows a principal sketch of the paths of incident recording pulses and cw-read-out beam with *s*−polarization, a modulation depth close to unity ($m \approx 1$), an average intensity $\bar{I} = (20.6 \pm 2.2)\,\mathrm{W/cm^2}$ (≡ peak intensity $I_0 = (3.9 \pm 0.6)\,\mathrm{TW/cm^2}$), and an intersection angle of $\Theta_B^{ext} = (6.8 \pm 0.2)°$. A continuous-wave He-Ne-laser served for

Optical Materials EXPRESS

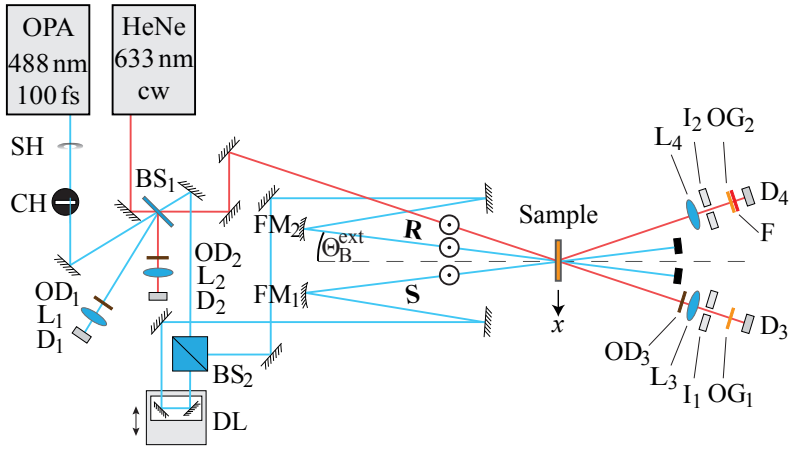

Fig. 5. Experimental setup for repetitive fs-pulse recording in BIQ-PDMS film samples. SH: shutter, CH: chopper (f_{rep} = 100 Hz), $FM_{1,2}$: focusing mirrors (f_{focus} = 500 mm), $BS_{1,2}$: beam splitters, $I_{1,2}$: iris diaphragm, $D_{1...4}$: diodes, $OD_{1...3}$: optical density filters, $OG_{1,2}$: orange glasses, F_1: single line filter, $L_{1...4}$: lenses, DL: delay line, R,S: reference and signal beams. The half angle between the two recording beams at λ_{record} = 488 nm is adjusted to $\Theta_B^{ext} = (6.8 \pm 0.2)^\circ$ that accords with a read-out angle $\Theta^{ext} \approx 8.8^\circ$ at λ_{read} = 632.8 nm.

Bragg-matched hologram read-out (λ_{read} = 632.8 nm, $\Theta^{ext} \approx 8.8^\circ$). Here, an average probe intensity of $I_0 = (350 \pm 30)\,mW/cm^2$ is used to minimize the probe-beam influence on the recording process.

3. Experimental results

3.1. In-Bragg read-out: cw-recording

Figure 6(a) shows the diffraction efficiency as a function of exposure $Q = (I_R + I_S) \times t$, i.e. the product of total recording intensity $I_R + I_S$ and time t, for the case of hologram recording with cw-laser light at 405 nm in OSO-PDMS films ($c = (0.36 \pm 0.03)$ mM) as an example.

The first-order diffraction efficiency shows a quadratic increase in the beginning of exposure ($Q < 0.2\,J/cm^2$). It passes a maximum value of $\eta_{max}^R = (2.75 \pm 0.64) \times 10^{-4}$ at an exposure of $Q_{max}^R = (0.91 \pm 0.06)\,J/cm^2$. Further exposure results in a monotonous decrease of the diffraction efficiency. The diffraction process disappears completely at exposures $> 10\,J/cm^2$. This behavior is comparable with the earlier findings in photoswitchable SNP crystals [15]. SNP also features a light-induced linkage isomerism related with the Fe-N-O-bond and two metastable states MS_1, MS_2 (Fe-O-N bond for MS_1 and a side-on-configuration of O-N with respect to Fe for MS_2) and the possibility for hologram recording. The dynamics in SNP (and further materials featuring reversible ground/metastable state optical systems) were explained considering the temporal evolution of the spatial concentration density [26]. We thus have applied the according generalized function

$$\eta(Q) = A \times I_1\,[m(Q - \delta Q)/Q_0]^2 \times \exp\,[-2(Q - \delta Q)/Q_0] \quad (1)$$

as fitting function for our experimental data. Here, $I_1(x)$ represents the modified Bessel function of the first kind and order as a function of x and δQ is an offset in exposure. The result of the fitting procedure is shown as solid line in Fig. 6a). A very large agreement between data and fit

Optical Materials EXPRESS

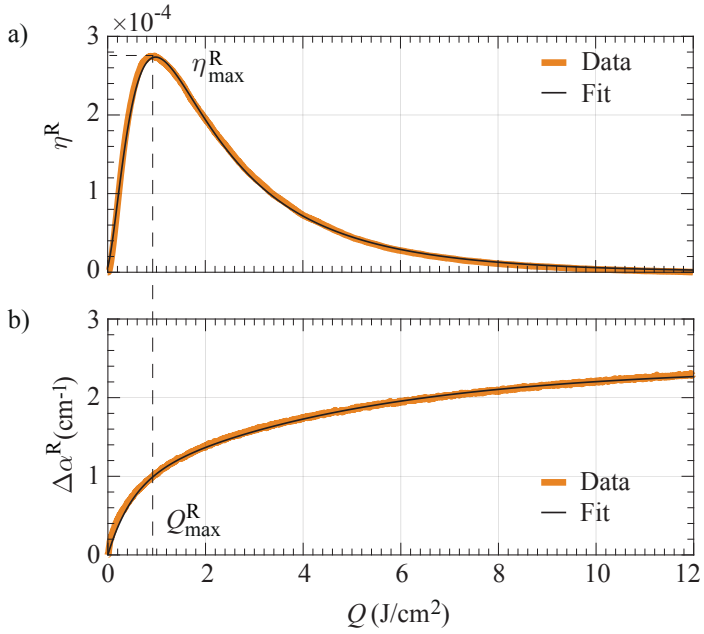

Fig. 6. **a)** Diffraction efficiency η^{R} (orange) as a function of exposure Q measured with a (0.36 ± 0.03) mM OSO-PDMS polymer film with a film thickness $d = (2.1 \pm 0.1)$ mm, and a fit (black) according to Eq. (1). A maximum value of $\eta^{R}_{max} = (2.75 \pm 0.64) \times 10^{-4}$ is reached at an exposure of $Q^{R}_{max} = (0.91 \pm 0.06)\,J/cm^2$. **b)** Light-induced change of the absorption coefficient $\Delta\alpha^{R}$ (orange) as a function of exposure Q, and a fit (black) according to the two-fold exponential function of Eq. (2) with characteristic exposures $Q_1 = (4.74 \pm 0.29)\,J/cm^2$ and $Q_2 = (0.49 \pm 0.11)\,J/cm^2$, respectively.

could be obtained with the amplitude A set to $(7.94 \pm 0.79) \times 10^{-3}$, $Q_0 = (0.77 \pm 0.08)\,J/cm^2$, $\delta Q = (0.05 \pm 0.01)\,J/cm^2$, and $m = (0.89 \pm 0.03)$. We note that $\eta^{R,S}(Q)$ were both detected during the hologram recording process. The analysis of the temporal dynamics $\eta^{S}(Q)$ yields similar values for $Q_0, \delta Q$, and m within the error margin of 10 %. Indications for the presence of the Borrmann effect were not found [27].

The sum of the intensities of zero and first order diffracted beams $I_\Sigma = I_t + I_d$ is used to simultaneously inspect the temporal evolution of the absorption change $\Delta\alpha(Q)$ by means of the Beer-Lambert law: $\Delta\alpha(Q) = -1/d \ln\left(I_\Sigma(Q)/I_\Sigma(Q=0)\right)$, as it is shown in Fig. 6(b). Our data set resembles the exponential growth reported for OSO-compound solvents in the work of Springfeld et al. [11] and Eicke et al. [28, 29]. A saturation value of $\Delta\alpha \approx 2.4\,cm^{-1}$ is reached at the end of exposure. The dynamics are best described by the sum of two exponential functions:

$$\alpha_{fit} = \alpha_0 + A_1 \exp(-Q/Q_1) + A_2 \exp(-Q/Q_2) \tag{2}$$

with $\alpha_0 = |A_1 + A_2|$ being the maximum change in absorption expected for $Q \to \infty$, and characteristic absorption and exposure $A_{1,2}$ and $Q_{1,2}$, respectively. This two-fold exponential function was originally introduced by Eicke et al. in order to take into account the significantly different lifetimes of the two O-bonded isomers MS_1, MS_2 at room temperatures [28, 29]: $\tau_1 \approx 1.6 \times 10^3$ s and $\tau_2 \approx 3.5 \times 10^4$ s [9]. Here, the outcome of the fitting procedure yields characteristic exposures of $Q_1 = (4.74 \pm 0.29)\,J/cm^2$ and $Q_2 = (0.49 \pm 0.11)\,J/cm^2$, i.e. a ratio $Q_1/Q_2 \approx 10$ ($A_1/A_2 \approx 1.8$, $A_1 = (-1.54 \pm 0.04)\,cm^{-1}$, $A_2 = (-0.85 \pm 0.02)\,cm^{-1}$).

We have repeated this type of measurements for OSO-PDMS samples with different OSO

Optical Materials EXPRESS

concentrations, while all other experimental parameters were kept largely identical (thickness $\bar{d} = (1.9 \pm 0.4)$ mm). Figure 7 shows the maximum obtained diffraction efficiency $\eta^{\mathrm{R}}_{\mathrm{max}}$ as a function of concentration c in the range up to about 1 mM. Throughout the investigated span, a

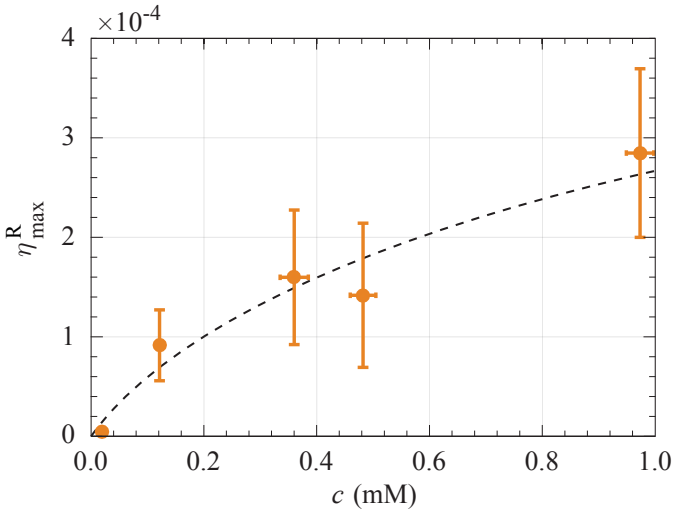

Fig. 7. Dependence of the maximum value of the diffraction efficiency $\eta^{\mathrm{R}}_{\mathrm{max}}$ as a function of OSO-concentration c in OSO-PDMS polymer films ($\bar{d} = (1.9 \pm 0.4)$ mm). An increase of $\eta^{\mathrm{R}}_{\mathrm{max}}(c)$ up to its threefold value is obvious. The dashed black line serves as a guide to the eye.

monotonous growth of $\eta^{\mathrm{R}}_{\mathrm{max}}$ as a function of concentration becomes obvious. In particular, it turns out that it becomes possible to tune the maximum efficiency up to a factor of about three by concentration management.

3.2. *Off-Bragg read-out*

Figure 8 shows the diffraction efficiency as a function of angular detuning $\Delta\Theta^{\mathrm{ext}}$ with respect to Bragg-incidence. The holographic grating under inspection has been recorded up to an efficiency of $\eta^{\mathrm{S}} = (1.21 \pm 0.23) \times 10^{-4}$ ($Q = (0.85 \pm 0.11)$ J/cm^2). The data set, often referred to as *rocking curve*, resembles the expected shape of a $\mathrm{sinc}^2(\Delta\Theta^{\mathrm{ext}})$ function. It shows a clear break-down of the diffraction efficiency for slight angular mismatches already in the order of 1/10 degree (Full width at half maximum, FWHM = $(0.18 \pm 0.01)°$). Remarkably, secondary and tertiary maxima can be resolved as well. The determined maximum value $\eta^{\mathrm{S}}_{\mathrm{max}}(\Delta\Theta^{\mathrm{ext}})$ slightly exceeds the value that was determined at the end of the grating recording process (η^{S}) by $\sim$ 15%. This may be attributed to the limitations in the experimental adjustment of the Bragg angle for read-out of about 0.1° that are in the order of magnitude of the FWHM of the grating's angular sharpness.

Nevertheless, the high quality of the experimental data set enables a fitting procedure using the original function $\eta(z, \Theta)$ as derived in Ref. [19] for lossy absorption gratings in accordance with Kogelnik's coupled wave theory [25]:

$$\eta(z,\Theta) = A_{\mathrm{LB}}(\Theta)\epsilon_1''(\lambda)^2 \frac{\left|\sinh\left(\frac{\left\{\epsilon_1''(\lambda)^2 - \left[2\beta(|\Theta|)\cos(\Theta)\epsilon_0'(\lambda)\right]^2\right\}^{1/2} k_0 z}{4\left[\epsilon_0'(\lambda)\right]^{1/2}\cos(\Theta)}\right)\right|^2}{\left|\left[2\beta(|\Theta|)\cos(\Theta)\epsilon_0'(\lambda)\right]^2 - \left[\epsilon_1''(\lambda)\right]^2\right|} \tag{3}$$

Optical Materials EXPRESS

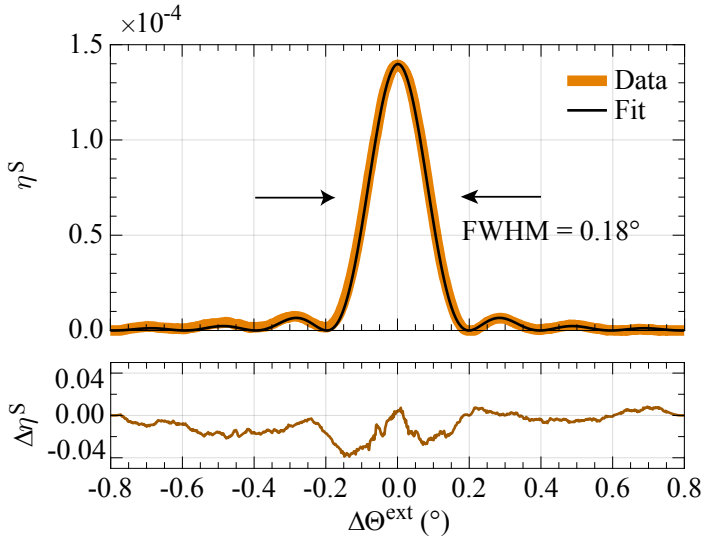

Fig. 8. Rocking curve as a function of deviation from the external Bragg angle $\Theta_B^{ext} = (6.4 \pm 0.2)^\circ$ for a (1.1 ± 0.1) mm thick (0.36 ± 0.03) mM OSO-PDMS sample after an exposure $Q = (0.85 \pm 0.11)$ J/cm^2 at $\lambda = (406.6 \pm 0.8)$ nm. The black line corresponds to the result of fitting Eq. (3) to the data set. Absolute deviations $\Delta\eta^S$ between data set and fitting result are shown below (identical decimal power).

with the abbreviations $A_{LB}(\Theta) = \exp[-\bar{\alpha}z/\cos(\Theta)]$ and $\beta(\Theta) = 2\sin(\Theta_B)^2/\cos(\Theta) - 2\sin(\Theta_B)\tan(\Theta)$. Here, z denotes the hologram thickness, Θ is the internally measured read-out angle with respect to the internal Bragg angle Θ_B, and $\bar{\alpha} = (\alpha_{GS}+\alpha_{MS})/2$ is the average absorption coefficient calculated from ground (GS) and metastable state (MS) absorption. The amplitude of the real permittivity grating is defined through $\epsilon_1''(\lambda) = \alpha_1 n_0/k_0$, where $\alpha_1 = (\alpha_{MS} - \alpha_{GS})/2$ is the modulation amplitude of the absorption coefficient, $\epsilon_0'(\lambda) = n_0^2$ is the average real permittivity or squared refractive index as a function of the wavelength, $k_0 = 2\pi/\lambda$ with λ the read-out wavelength. We note that the presence of a lossy absorption grating is well justified by the experimentally determined pronounced change of the absorption coefficient as a function of light exposure, as depicted in Fig. 6.

The result of the fitting procedure is depicted in Fig. 8 by the solid black line. A very good agreement between fit and data set is obtained for a hologram thickness $z = (690 \pm 10)\,\mu$m and the fitting parameters summarized in Table 1.

Table 1. Parameters obtained from fitting the theoretical function of a rocking curve for the case of a lossy grating (Eq. (3)) to the experimental data set (cf. black line in Fig. 8).

fitting parameters	
fixed	open
$\lambda = 532$ nm	$n_0 = (1.35 \pm 0.05)$
$\alpha_{GS} = (1.17 \pm 0.05)\,\text{cm}^{-1}$	$\Theta_B = (4.73 \pm 0.35)^\circ$
$\alpha_{MS} = (2.63 \pm 0.05)\,\text{cm}^{-1}$	$z = (690 \pm 10)\,\mu$m

Optical Materials EXPRESS

3.3. Angular multiplexing

The previous section reveals the angular dependence of the diffraction efficiency for one hologram written into the OSO-PDMS-sample. In a next step, taking into account the FWHM, several holograms can be written within the same volume without any crosstalk between the gratings. This technique is called angular multiplexing and is crucial for evaluating the suitability of materials towards high information storage densities and therefore mass data storage applications.

Figure 9 shows the result of angular read-out after the recording of four individual volume holograms within (nearly) the same volume element of an OSO-PDMS film (concentration $c = (0.36 \pm 0.03)$ mM, thickness $d = (2.1 \pm 0.1)$ mm) by means of in-plane angular multiplexing [16, 17]. Recording of each holographic grating within the sequence #1...#4 was performed analogously to the scheme presented in the previous section. Here, an exposure of up to $Q = (1.2 \pm 0.2)$ J/cm^2 was used for a single hologram. At the end of each recording process, the film was rotated in the dark by predefined angular steps of 1.0°, i.e. by an angle far exceeding the FWHM of a single grating (cf. Fig. 8). Diffraction of the recording beams at previously recorded gratings therefore was suppressed. After the recording of all four holograms within the same volume element, the data set of Fig. 9 was obtained by read-out with the probe beam I_0^R ($\lambda = 532$ nm) during film rotation at constant velocity (0.01°/s) over the angular range from -1° to +4°. The diffracted signals appear with clear angular separation of about 1° and without the appearance of mutual interaction or of ghost images. The first hologram features a maximum diffraction efficiency of $\eta^R_{max} = (1.97 \pm 0.38) \times 10^{-5}$ that is reduced by about 25% with increasing hologram number.

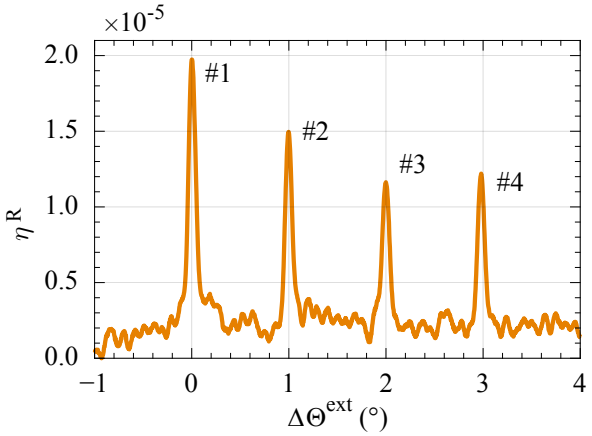

Fig. 9. Four holographic gratings have been written into a (0.36 ± 0.03) mM OSO-PDMS sample with a thickness $d = (2.1 \pm 0.1)$ mm and with a mutual angular mismatch of 1° in the sequence #1...#4. Recording for each hologram was stopped at an exposure of $Q = (1.2 \pm 0.2)$ J/cm^2. At the end of the entire recording scheme, read-out was performed with the probe beam I_0^R ($\lambda = 532$ nm) during film rotation at constant velocity (0.01°/s) over the angular range from -1° to +4°.

3.4. In-Bragg read-out: fs-pulse recording

Figure 10 shows the result for hologram recording in BIQ-PDMS polymer films using repetitive fs-pulse exposure ($f_{rep} = 100$ Hz). The diffraction efficiency is shown as a function of average exposure $\overline{Q}$ that here is determined by the product of average intensity $\overline{I}$ and time t. The data set was obtained with a BIQ-PDMS film at a recording wavelength $\lambda_{record} = 488$ nm. A Bragg

Optical Materials EXPRESS

angle $\Theta_B^{ext} = (6.8 \pm 0.2)°$, *s*-polarization and average intensity of $\overline{I} = (20.6 \pm 2.2)\,W/cm^2$ were chosen. Bragg-matched read-out was performed with a HeNe laser beam at $\lambda_{read} = 632.8\,nm$ ($\Theta^{ext} \approx 8.8°$).

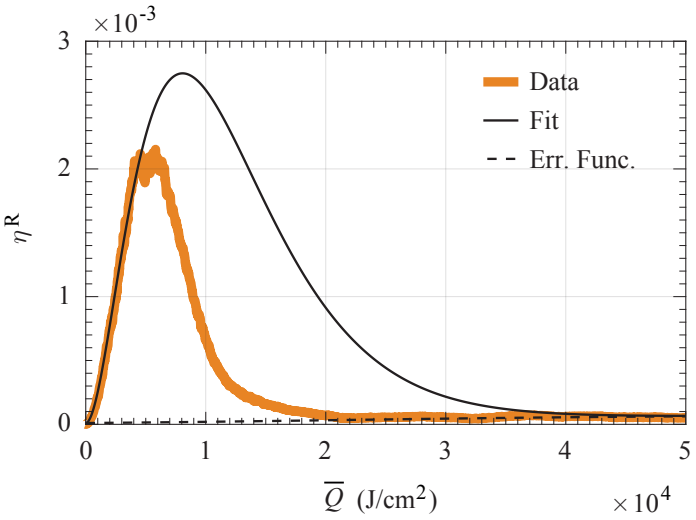

Fig. 10. Diffraction efficiency (orange) as a function of average exposure using a (1.86 ± 0.03) mM BIQ-PDMS sample with a thickness $d = (1.3 \pm 0.1)$ mm for the particular case of repetitive fs-pulse exposure ($f_{rep} = 100$ Hz). The fit (black solid line) according to Eq. (1) for $0 < \overline{Q} < 0.4 \times 10^4$ J/cm^2 requires an additional term modeled by a Gauss error function (black dashed line). A maximum value of $\eta^R_{max} = (2.0 \pm 0.1) \times 10^{-3}$ is reached at an average exposure of $\overline{Q}^R_{max} = (5.3 \pm 1.3) \times 10^3$ J/cm^2.

The data set shows a temporal evolution of $\eta^R(\overline{Q})$ that is qualitatively comparable with the cw-recording case for OSO-PDMS films. The initial increase follows a quadratic dependence. A striking maximum of $\eta^R_{max} = (2.0 \pm 0.1) \times 10^{-3}$ is reached for $\overline{Q}^R_{max} = (5.3 \pm 1.3) \times 10^3$ J/cm^2. Thereafter, $\eta^R(\overline{Q})$ decreases significantly as a function of average exposure. There are three obvious differences with respect to cw-recording: (i) the maximum value $\eta^R_{max}(\overline{Q}^R_{max})$ exceeds the respective value for the case of cw-recording by nearly a factor of ten compared to OSO, (ii) the diffraction efficiency remains constant as a function of average exposure between 4.0×10^3 J/cm^2 and 6.6×10^3 J/cm^2, i.e. upon reaching the maximum, and (iii) a saturation value of $\eta(\overline{Q} \to \infty) \approx 6.9 \times 10^{-5}$ remains even for very large average exposure ($\overline{Q} \gg 10^4$ J/cm^2), i.e. light in direction of the reconstructed beam cannot be erased completely. As a result, the fitting function as defined via Eq. (1) requires an additional term modeled by a Gauss error function (black dashed line). Furthermore, successful fitting of the data set becomes only possible for low average exposure ($\overline{Q} \ll 1 \times 10^4$ J/cm^2). The solid black line in Fig. 10 represents the outcome of the fitting procedure within the limits of $0 < \overline{Q} < 0.4 \times 10^4$ J/cm^2 (fit parameters: $A = (2.8 \pm 0.5)$, $Q_0 = (0.80 \pm 0.04) \times 10^4$ J/cm^2, and $m = 0.17 \pm 0.04$). An overestimation of $\eta(\overline{Q})$ for $\overline{Q} \gg 0.5 \times 10^4$ J/cm^2 is self-evident.

The data set is further used to estimate the rise in the diffraction efficiency during a single fs-pulse event. A value of $\eta_{pulse} = (1.26 \pm 0.16) \times 10^{-7}$ is obtained by considering a pulse duration of 100 fs, a total average recording intensity of $\overline{I} = (20.6 \pm 2.2)\,W/cm^2$, i.e. a single fs-laser-pulse exposure of $\overline{Q}_{100\,fs} = (0.21 \pm 0.02)$ J/cm^2, and the value of the gradient $\delta\eta/\delta\overline{Q}$. The latter was determined from the experimental data set in the regime of monotonous growth at

Optical Materials EXPRESS

$\overline{Q} \approx 3,000\,\mathrm{J/cm^2}$.

4. Discussion

4.1. Holographic performance of ruthenium sulfoxide complexes

Our results allow for a reliable evaluation of the performance of OSO-PDMS and BIQ-PDMS polymer films as holographic recording media. The holographic studies and the material synthesis approach aim at a discussion of predominantly consumer-market holographic applications such as (real-time) 3D holographic imaging [30, 31] or holographic mass data storage [32, 33]. In what follows, we will first discuss the individual results of our holographic analysis. Then, we will focus on a comparison of our data with SNP, that we regard as reference material system with embedded molecular switches. Finally, based on the discussed issues, we will tackle the question about the origin of the poor diffraction efficiency, i.e. on how to improve it for modern holographic applications.

4.1.1. Dynamics of the hologram diffraction efficiency

Let us first focus on the main features of the holographic polymer films: Unambiguously, our results verify the possibility of hologram recording in as-prepared OSO-PDMS and BIQ-PDMS polymer films by using either cw- and femtosecond pulse-train exposure at wavelengths in the blue-green spectral range. Independent on the light source, the recording process follows the well-known temporal evolution of the diffraction efficiency as a function of exposure for an optical system with two addressable states and exposure with a sinusoidal intensity pattern [26]. The rise and subsequent decay of the diffraction efficiency represents the temporal evolution of the modulation depth of the recorded hologram. The transient feature is a result of the fact that the population of the states $MS_{1,2}$ is exclusively dependent on the exposure, and not on the intensity. Therefore, saturation population can be reached even in the regions of the fringe pattern with very low light intensity. The quality of reconstruction of $\eta(Q)$ for the cw-case using the fitting function Eq. (1) as derived in the original work of Fally et al. [26] is very remarkable. Furthermore, the determined rise of the absorption change as a function of exposure is in full agreement with literature data. It represents the clear dependence of the population, being proportional to the absorption change via the absorption cross-section, on the exposure under cw-laser light illumination. It can be successfully fitted using a two-exponential function which has been investigated systematically by Eicke et al. [28, 29] in the framework of two individually addressable metastable states $MS_{1,2}$ as well as the nearly collinear geometry of the pump-probe beams.

A similar statement on the dynamics of $\eta(Q)$ is possible for the recording with a fs-laser pulse train in BIQ-PDMS polymer films. However, the temporal evolution can be reconstructed with sufficient quality within the limits of a low average exposure, i.e. prior to reaching the maximum of η. We here note that the average exposure required for sufficient hologram recording is by three orders of magnitude larger in direct comparison with the cw-recording case. This can be attributed to: i) the photosensitivity of BIQ-sulfoxides is by nearly a factor of 10 smaller than for OSO [28] and ii) the fs-pulse train exposure used for the study of BIQ-PDMS polymer films cannot be compared straightforwardly with the cw-recording case applied for the OSO-PDMS polymer film. In particular, we here use femtosecond laser pulses with pulse durations that are below the typical rise time of linkage isomerism in sulfoxide compounds (usually in the order of 200 ps [23]). Thus, this pulse duration is sufficient to trigger an instantaneous metal-to-ligand-charge-transfer (MLCT) via Franck-Condon's principle, but it is much shorter than the lifetime of the molecule in the excited (transient) state. As a result, relaxation of the excited molecule is solely driven by the principle of energy minimizing. Repetitive excitation, as it may occur in the case of pulse durations much larger than 200 ps or cw-exposure, must be excluded and may be a reason

Optical Materials EXPRESS

for the decelerated population of metastable states as a function of average exposure. The observation of a plateau value of η in its maximum may be attributed to stability limits of our setup. Furthermore, this may explain the decrease of η to a non-zero saturation value. The very low value of the diffraction efficiency most probably points to the presence of light-scattering, e.g. due to parasitically recorded holograms [34, 35], and/or the generation of laser-induced damage at the sample's surface.

4.1.2. Hologram thickness

From the optics viewpoint, OSO-PDMS and BIQ-PDMS polymer films feature a very high quality of the recorded holograms as represented by the experimental results of the rocking curve in Fig. 8. The fit function for off-Bragg read-out as derived from Kogelnik's formula for an unslanted lossy grating [19, 25] shows excellent agreement with the experimental data. This high quality of the data set allows for a straight-forward analysis of the recorded absorption hologram. We obtain a hologram thickness of $z \approx 690\ \mu$m that is by about 40% lower than the film thickness of 1.1 mm. The hologram therefore has not been recorded within the entire volume of the polymer film. It is very likely to attribute this finding to geometrical factors taking into account the widths of the recording beams and the internal intersection angle. Larger hologram thicknesses thus may be obtained by larger beam diameters that, however, require a recording laser with increased power.

4.1.3. Hologram multiplexing

The appearance of the higher-order side-maxima needs to be considered in the framework of recording multiple holograms. We here successfully demonstrate the recording of four individual holograms using angular multiplexing. The appearance of ghost images could be suppressed using intermediate angular steps of about 1°. Both, the FWHM of the rocking curve of $\approx 0.2°$ and the intermediate step width strongly limit the number of multiplexed holograms in the film under investigation. This limit may also be overcome by choosing larger hologram thicknesses that considerably reduce the FWHM of the rocking curve, i.e. it then becomes possible to reduce the intermediate angular step width.

4.1.4. Hologram recording with fs-pulse trains

The possibility of hologram recording with fs-pulse trains is of major importance considering the market growth of low-cost, high-power sub-picosecond laser systems. Furthermore, the possibility of an efficient hologram within a single laser pulse event is of interest for rapid changes of hologram images. In crystalline systems, single-pulse recording was demonstrated in lithium niobate, $LiNbO_3$, where a diffraction efficiency of more than 10 % was reached within an 8 ns laser pulse [36]. Moreover, fs-pulse recording was also successful in SNP single crystals. The possibility of fs-pulse recording therefore is another striking feature of OSO-PDMS and BIQ-PDMS polymer films that could be demonstrated with our study. This feature reflects the ultrafast response of the molecular switching process. However, in order to reach a maximum efficiency, a large concentration of OSO- and BIQ-molecules in the metastable states is desired that requires a fs-pulse train over an extended time range.

4.1.5. Limitations of the hologram diffraction efficiency

All these features so far point to an outstanding performance of OSO-PDMS and BIQ-PDMS polymer films. A severe disadvantage of these materials, however, is related to the maximum reached diffraction efficiency. Already, in the first proof-of-principle reports of elementary holograms in similar OSO-PDMS samples, η-values of up to $\approx 8 \times 10^{-6}$ were reported [14]. Our study here shows very remarkably that it is possible to improve this value by adjusting the OSO concentration, etc., and the use of a professional two-beam interferometer by a factor

Optical Materials EXPRESS

of about 100. Nevertheless, we were not able to exceed values of $\sim 10^{-3}$ for η in any of our samples and experimental conditions. A further possibility to enhance η would be by increasing the hologram thickness z. Considering Eq. (3) and the given experimental conditions, a rise by a factor of 10 may be reasonable for this particular case by adjusting $z \approx 11$ mm and for the OSO concentration under study. However, all these efforts will not be satisfying from the viewpoint of any application.

4.2. Comparison with crystalline holographic materials based on photoswitchable compounds

4.2.1. Holographic performance and material properties

Several advantages of OSO-PDMS and BIQ-PDMS polymer films reflected by the further studies become obvious when compared to crystalline photoswitchable compounds used for hologram recording in recent years. The most prominent candidate is sodium nitroprusside, $Na_2[Fe(CN)_5NO]\cdot 2H_2O$, (SNP). The single crystals will now serve as reference material for our further discussion due to their outstanding properties including the possibility for reaching diffraction efficiencies of up to 100% ($\eta = I_d/(I_t + I_d)$) due to large light-induced index changes of up to $\delta n \sim 10^{-2}$. SNP is also very similar to OSO-PDMS and BIQ-PDMS films with respect to its spectral sensitivity of the population process of both metastable states $MS_{1,2}$ using blue-green laser light.

The general holographic features can be well compared: The diffraction efficiency of SNP shows a transient evolution in full accordance with the results presented in this contribution for OSO-PDMS and BIQ-PDMS and were analyzed in detail in Ref. [26]. Off-Bragg read-out revealed similar rocking curves as for ruthenium sulfoxide polymers, though higher-order side maxima of the rocking curve (Fig. 8) were experimentally not observed. A reason is the comparably large fundamental absorption of SNP at the read-out wavelengths. Recording of up to eight holograms was verified within the same volume in 200μm thin plates of SNP [34].

Despite these holographic similarities, the materials themselves and their photofunctional properties are rather different: The synthesis of SNP requires a time-consuming crystal growth procedure from aqueous solution and polishing to optical quality. For recording of long-lived holograms ($\gg 100$)s, SNP samples need to be cooled below 200 K [15, 34]. For comparison, the relaxation dynamics of the metastable states $MS_{1,2}$ in ruthenium sulfoxide complexes possess lifetimes in the order of hours at room temperature [9], thus imposing holographic grating lifetimes at a similar temporal scale. Moreover, the dimensions of SNP crystals remain limited to sizes of a few square centimeters. The large density of NP compounds within the crystalline matrix limits the crystal thickness to a few 100 μm for optical experiments due to pronounced absorption in the visible spectrum. On the contrary, the synthesis of OSO-PDMS polymer films and BIQ-PDMS polymer films can be realized on a large scale with sufficient optical quality. It is possible to carefully adjust the transmission loss by concentration tuning. A further striking advantage is the mechanical flexibility of the films [4]. This particularly widens the range of possible applications, e.g. for integrated head-up displays in curved windshields.

4.2.2. Diffraction efficiency

The striking similarities of the underlying photophysics in OSO-PDMS polymer films and SNP single crystals require a more fundamental discussion on the exceedingly different values of the diffraction efficiency in these two systems (about 10^{-4} in OSO-PDMS and 10^{-3} in BIQ-PDMS compared with up to 1 in SNP). One attempt to explain the measured small efficiency may be related to a small concentration of molecules in our film samples. We limit the concentration to $c \leq 1.0$ mM (OSO-PDMS) and $c \approx 1.9$ mM (BIQ-PDMS) in order to counterbalance diffraction efficiency against fundamental absorption. In SNP, the density of photoswitchable compounds is comparably large (4 molecules per unit cell) due to their role as building blocks in the

Optical Materials EXPRESS

crystallographic system and up to 50% of the ground state molecules may be switched to MS_1. Our results show that in OSO, η can be increased with growing concentration in our polymer films and it becomes possible to obtain a rise of η by a factor of three. However, concentration-dependent tuning by a factor of more than 1,000 seems not very likely.

The fs-pulse train investigation allows for a more detailed comparison between the diffraction efficiencies of OSO- and BIQ-PDMS polymer films and SNP single crystals, in particular if we consider the rise of the diffraction efficiency upon a single pulse event. For SNP it was already shown that single-pulse exposure with pulse durations of 4 ns reveal strongly limited values of $\eta \approx 10^{-4}$ [37]. We here demonstrate that BIQ-PDMS polymer films allow for hologram recording with $\eta \approx 1.3 \times 10^{-7}$ within a single sub-ps laser pulse event. For comparison with an average exposure of about 1 ns a diffraction efficiency of $\eta \approx 10^{-4}$ may be reached after about 10,000 consecutive 100 fs laser pulses. This shows that the efficiency in a single-pulse recording step is quite comparable between SNP single crystals and BIQ-PDMS polymer films. While consecutive single-pulse recording is capable to increase the diffraction efficiency by a factor of ten in comparison to the *cw*-recording case (cf. Fig. 8), we were not able to determine η values of more than $\approx 10^{-3}$ for any experimental condition.

4.3. *Holographic performance: the role of symmetry and order of photoswitchable compounds*

It is very likely to assume that OSO-PDMS and BIQ-PDMS polymer films generally reveal diffraction efficiencies that are far below any relevance for holographic applications. By comparison with the SNP reference system the main reason most probably may be attributed to the structural disorder of the OSO- and BIQ-molecules. In single crystalline SNP two photoswitchable compounds are oriented contrariwise within each *a*-*b*-mirror plane of the orthorhombic unit cell and with about ±45° to the *a*-axis alternating along the *c*-axis [38]. This symmetry is conserved even in the metastable state, i.e. there are no hints for a light-induced structural phase transition. On the contrary, it is solely a result of the N-O-inversion, i.e. a rotation of the N-O-bond by about 180° with respect to the Fe-N-O axis (MS_1). The symmetry may be responsible for a major contribution of light-induced index changes with the photo-induced structural changes of the nitrosyl compound. This already was experimentally verified and discussed in Ref. [39] from the viewpoint of related changes of the molecular polarization. The pronounced and periodic alteration of the local structure of the molecular crystal adds up to major changes of the index of refraction of up to 10^{-2}. The use of thin crystalline plates of $\approx 200\mu$m is sufficient for elementary grating recording with efficiencies of up to 100%. The crystallographic feature particularly is reflected in the dependence of recording and read-out polarizations with respect to the crystallographic axis, but furthermore in the possibility for grating recording with mutually orthogonal polarized laser beams in SNP [15, 18, 39].

The high symmetry and order of the photoswitchable compounds is clearly missing in OSO-PDMS and BIQ-PDMS (and any other PDMS-based polymer film based on photoswitchable compounds). Thus, the major contribution to the grating recording process is the optically induced change of the molecular absorption which is directly determined by the population of molecules in the ground and/or excited state (depending on the probe wavelength). Kramers-Kronig relation demands for the causal consideration of an additional contribution of the index of refraction as discussed in Ref. [13] with $\eta \approx 10^{-6}$. In other words, a contribution from a pure index grating is negligible and thus supports the applicability of Eq. (3). Taking into account the limits of the diffraction efficiency of lossy gratings ($\approx 3.7\%$ following Kogelnik's definition for η [25]), it does not reveal any potential for breathtaking results.

On the contrary, it may be very promising to foster further material scientific efforts with the goal to synthesize OSO- or BIQ-PDMS polymer films with an intrinsic structural order. The latter may be inspired by the SNP model system, i.e. the director of structural change of

Optical Materials EXPRESS

the individual molecule may be oriented anti-parallel to each other within a single layer and all molecules may be aligned layer by layer. This may be reached by promising approaches of synthetic crystallography also including organic chemistry. Though potentially promising, the aspect of keeping synthesis at low cost must be considered carefully in the framework of consumer applications. Also, any structural approach may be connected with losing the material's softness of the polymer film.

5. Conclusion

An outstanding performance of OSO-PDMS and BIQ-PDMS polymer films is reflected by the dynamics of the efficiency, the quality of the off-Bragg read-out of the recorded holographic elementary lossy gratings, the possibility for angular multiplexing as well as the recording with continuous-wave and even a fs-laser pulse train at room temperature. These features already indicate some of the most important aspects for achieving high holographic storage densities. Together with its mechanical and tuning flexibility, e.g. concentration, as well as the scalability at a low-cost and short-time synthesis process provides a competitive advantage over established materials for holographic information storage. These advantages, however, remain limited by maximum values of the diffraction efficiencies of up to $\sim 10^{-3}$. Further tuning by means of adjustment of molecular concentration, holographic grating thickness, recording parameters, etc. fail to overcome this threshold value. In comparison to single crystalline reference media, it can be concluded that the structural disorder of the photoswitchable molecules is at the origin of this limitation. It may be overcome by targeted synthesis of polymer films with oriented and structurally ordered sulfoxide compounds. Then, however, the question about synthesis costs and lack of mechanical flexibility will represent well-known challenges of holographic media based on photoswitchable compounds.

Funding

Deutsche Forschungsgemeinschaft (DFG) (INST 190/165-1 FUGG); Open Access Publishing Fund of Osnabrueck University.

Acknowledgments

We particularly express our thanks to Jeffrey J. Rack and his research group, including Maksim Livshits, from the university of Albuquerque (New Mexico, United States of America) for providing the OSO- and BIQ-sulfoxide compounds for our study. We thank Sebastian Eicke, Kristin Springfeld, Volker Dieckmann and Holger Badorreck for discussion.